A convolutional sparsity regularization for solving inverse scattering problems

Rencheng Song *Member, IEEE*, Qiao Zhou, Yu Liu *Member, IEEE*, Chang Li *Member, IEEE* and Xun Chen, *Senior Member, IEEE*

***Abstract*—In this letter, a convolutional sparsity regularization (CSR) is introduced into the framework of nonlinear iterative methods for solving inverse scattering problems (ISPs). The permittivity image of scatterers is sparsely represented in a convolutional form with pre-learned dictionary filters. The CSR is then incorporated with the subspace-based optimization method (SOM), termed as (SOM-CSR), to reconstruct the target image as a sparse coding by dictionary filters. The whole optimization function of SOM-CSR is solved using an alternative iteration method. Both synthetic and experimental data are employed to validate the effectiveness of the proposed SOM-CSR method. The results demonstrate that the CSR, as a structural constraint, is beneficial to nonlinear iterative reconstruction methods for solving ISP in contrast to pixel-based inversion.**

***Index Terms*—Electromagnetic inverse scattering, convolutional sparse coding, sparsity regularization.**

I. Introduction

Electromagnetic inverse scattering problems (ISPs) aim to reconstruct the geometry, position, and physical properties of unknown scatterers from measured scattered fields. The ISP reconstruction has been widely required in biomedical imaging, non-destructive testing, and remote sensing, etc. Due to the inherent ill-posedness and nonlinearity, it is challenging to achieve a stable and efficient reconstruction of ISP.

The full-wave ISP is usually solved by nonlinear iterative methods, such as the Levenberg-Marquardt method (LM) [1], the distorted Born iterative method (DBIM) [2], [3], the contrast source inversion method (CSI) [4], [5], and the subspace optimization method (SOM) [6], to overcome the ill-posedness and nonlinearity issues. These methods typically linearize nonlinear ISPs by simplifying the model with approximations or taking alternating optimization to decouple parameters. Meanwhile, regularization terms are implemented to stabilize the reconstruction [7] for dealing with ill-posedness. The regularization aims to add constraints to the searching space of optimization. The prior information related to physical laws, geometrical knowledge, or some other reasonable assumptions on unknown scatterers can all be incorporated to define the regularization terms.

In recent years, sparse representation (SR) of unknown scatterers has become a popular kind of structural regularization to solve ISPs in low-dimensional models. For example, Desmal et al. [8]–[10] introduced a sparse constraint on pixels of permittivity and induced current images with l^1-norm, which means the contrasts of target need to be nonzero only within a small portion in the domain of interest (DOI). Besides the pixel-wise SR, the unknowns of scatterers can also be sparsely represented with mathematical basis functions [11]–[13]. The basis-based SR can represent the scatterer in a much more sparse manner in comparison to the pixel-wise one. However, the performance of basis-based SR strongly depends on the selected basis functions, which may lack adaptability to different types of scatterers. The pixel-wise and basis-based low-dimensional SR models can be solved in a popular way under the framework of compressive sensing (CS) [14]–[16]. For more details about the applications of CS in ISP, the readers can refer to review papers [17], [18].

In this letter, we introduce a convolutional sparsity regularization (CSR) into the framework of nonlinear iterative methods for solving two-dimensional (2-D) ISPs. The SOM, as a representative nonlinear ISP method, is used to demonstrate the principle of the algorithm. The proposed method, named SOM-CSR, first represents the unknown scatterers by the convolutional sparse coding (CSC) [19] with pre-learned dictionary filters. The convolutional sparsity representation is then incorporated into the SOM as a sparsity constraint to deal with the ill-posedness of ISP through restricting structural information of targets. The cost functions are alternatively optimized among the contrast, ambiguous induced current, and the sparse coding coefficients. The effectiveness of the CSR is evaluated with both synthetic and experimental data, where the results demonstrate the benefit of this regularization to enhance the reconstruction quality.

Compared with other sparsity regularization, the proposed CSR has the following advantages.

1) It makes better use of the prior structural information of scatterer images through the convolutional dictionary learning. To the best knowledge of the authors, the learned dictionary is used for the first time to solve ISPs. This makes it easy to incorporate prior information to restrict the solution space, thereby reducing the ill-posedness of the problem.

This work was supported in part by the Anhui Key Project of Research and Development Plan (Grant 202104d07020005), the National Natural Science Foundation of China (Grants 61922075, 41901350), the Provincial Natural Science Foundation of Anhui (Grant 2008085QF285), and the Fundamental Research Funds for the Central Universities (Grants PA2021KCPY0051 and JZ2021HGTB0078). (Corresponding author: Yu Liu).

R. Song, Q. Zhou, Y. Liu and C. Li are with the Anhui Province Key Laboratory of Measuring Theory and Precision Instrument, and also the Department of Biomedical Engineering, Hefei University of Technology, Hefei 230009, China (e-mail:rcsong@hfut.edu.cn; zhouqiao@mail.hfut.edu.cn; yuliu@hfut.edu.cn; changli@hfut.edu.cn).

Xun Chen is with the Department of Electronic Engineering and Information Science, University of Science and Technology of China, Hefei, Anhui, 230001, China (e-mail: xunchen@ustc.edu.cn).

2) In CSC, the SR is obtained over the whole image, rather than independently computing the representations for a set of overlapping small patches in conventional SR [20]. This coding manner, which ensures the global correlation of the scatterer image, can reconstruct the local structure of unknown scatterers in a more robust way, so as to improve the reconstruction quality of the ISP.

The structure of this letter is as follows. Section II introduces the proposed method. Section III presents the numerical examples and related results. Finally, we make conclusions in Section IV.

II. Method

A. Forward problem

A 2-D ISP is considered with the transverse magnetic polarization. The unknown non-magnetic scatterers are located in the DOI D with a free-space background. There are N_t transmitters and N_r receivers at a circle S surrounding D, respectively. The forward scattering is governed by the Lippmann-Schwinger equations [7]. Suppose the DOI D is discretized into P small subunits. The total electric field $\mathbf{E}^{tot}$ in D satisfies the following formula

$$\mathbf{E}^{tot} = \mathbf{E}^{inc} + \mathbf{G}_D \cdot \boldsymbol{\xi} \cdot \mathbf{E}^{tot}, \tag{1}$$

where $\mathbf{E}^{inc}$ denotes the incident electric field, $\boldsymbol{\xi}$ is the contrast, and $\mathbf{G}_D$ indicates the 2-D free-space Green's function mapping from the induced current $\mathbf{I} = \boldsymbol{\xi} \cdot \mathbf{E}^{tot}$ to the scattered field in D.

Meanwhile, the scattered field $\mathbf{E}^{sca}$ in the domain of measurement S can be expressed as

$$\mathbf{E}^{sca} = \mathbf{G}_S \cdot \boldsymbol{\xi} \cdot \mathbf{E}^{tot}, \tag{2}$$

where $\mathbf{G}_S$ is the 2-D free-space Green's function mapping from the induced current in D to the scattered field at S.

B. Convolutional sparsity regularization

The purpose of ISP is to retrieve the permittivity contrast $\boldsymbol{\xi}$ from scattered field $\mathbf{E}^{sca}$. As is well known, $\boldsymbol{\xi}$ has relation with the relative permittivity $\boldsymbol{\epsilon}_r$ as $\boldsymbol{\xi} = -i(k/\eta_0)(\boldsymbol{\epsilon}_r - 1)$, where k and η_0 are the wavenumber and the impedance in the free space, respectively, and $i = \sqrt{-1}$.

The dictionary filters and the corresponding CSC of permittivity images can be solved in a unified manner as

$$\begin{aligned} \underset{\{\mathbf{d}_m\},\{\mathbf{x}_{l,m}\}}{\arg\min} \ & \frac{1}{2}\sum_{l=1}^{L} \| \sum_{m=1}^{M} \mathbf{d}_m * \mathbf{x}_{l,m} - \boldsymbol{\epsilon}_{r,l}\|_2^2 + \\ & \lambda \sum_{l=1}^{L}\sum_{m=1}^{M} \|\mathbf{x}_{l,m}\|_1, \text{such that } \|\mathbf{d}_m\|_2 = 1, \end{aligned} \tag{3}$$

where $\{\mathbf{d}_m\}_{m=1}^M$ are M convolutional dictionary filters with size $N_f \times N_f$, $\boldsymbol{\epsilon}_{r,l}$ is the lth permittivity image to be coded, $\{\mathbf{x}_{l,m}\}_{m=1}^M$ are the M unknown sparse coding maps of $\boldsymbol{\epsilon}_{r,l}$, $\|\cdot\|_2$ indicates the l^2 norm, $\|\cdot\|_1$ denotes the l^1 norm, * represents convolution operation, and λ is the regularization parameter. The unitary constraint on the l^2 norm of filters aims to avoid the scaling ambiguity of coding coefficients.

In Eq. (3), the unknown $\{\mathbf{d}_m\}_{m=1}^M$ and $\{\mathbf{x}_{l,m}\}_{m=1}^M$ can be solved alternatively by the augmented Lagrangian methods [21] with efficient solution of the main linear systems [22]. The above algorithms are implemented with the open-source code 'SPORCO' [23].

In this paper, we first obtain $\{\mathbf{d}_m\}_{m=1}^M$ with a set of given permittivity images $\{\boldsymbol{\epsilon}_{r,l}\}_{l=1}^L$. The filters $\{\mathbf{d}_m\}_{m=1}^M$ are considered to learn prior structural information of target scatterers. In the ISP, the unknown $\boldsymbol{\epsilon}_r$ can then be represented by the CSC with given $\{\mathbf{d}_m\}_{m=1}^M$, which performs as the convolutional sparsity regularization (CSR). The implementation details are introduced next under the framework of SOM.

C. SOM-CSR

The SOM method takes the state equation as a physical regularization, and it further decouples the induced current $\mathbf{I}$ into the deterministic ($\mathbf{I}^s$) and the ambiguous ($\mathbf{I}^a$) parts to remedy the illposedness [6]. In the proposed SOM-CSR, the CSC in Eq. (3) is easily incorporated into the framework of SOM, as a structural regularization term. The full optimization function of SOM-CSR is

$$\begin{aligned} \underset{\boldsymbol{\xi},\{\boldsymbol{\alpha}_j\},\{\mathbf{x}_m\}}{\arg\min} \ & \frac{1}{2}\sum_{j=1}^{N_t}\left(\frac{\|\mathbf{G}_S\cdot\mathbf{V}\cdot\boldsymbol{\alpha}_j + \mathbf{G}_S\cdot \mathbf{I}_j^S - \mathbf{E}_j^{sca}\|_2^2}{\|\mathbf{E}_j^{sca}\|_2^2} + \frac{\|\mathbf{A}\cdot\boldsymbol{\alpha}_j - \mathbf{B}_j\|_2^2}{\|\mathbf{I}_j^s\|_2^2}\right) \\ & + v\left(\frac{1}{2}\|\sum_{m=1}^{M}\mathbf{d}_m * \mathbf{x}_m - \boldsymbol{\epsilon}_r\|_2^2 + \lambda\sum_{m=1}^{M}\|\mathbf{x}_m\|_1\right), \end{aligned} \tag{4}$$

where $\mathbf{A} = \mathbf{V} - \boldsymbol{\xi}\cdot(\mathbf{G}_D\cdot\mathbf{V})$, $\mathbf{B}_j = \boldsymbol{\xi}\cdot\left(\mathbf{E}_j^{inc} + \mathbf{G}_D\cdot\mathbf{I}_j^s\right) - \mathbf{I}_j^s$, $\mathbf{V}$ denotes the noise space composing by the last few singular vectors of $\mathbf{G}_S$, $\boldsymbol{\alpha}_j$ is the corresponding coefficient vector of the ambiguous induced $\mathbf{I}_j^a$, and v is the regularization parameter to balance the SOM and the CSR.

The parameters $\boldsymbol{\xi}$, $\{\boldsymbol{\alpha}_j\}$ and $\{x_m\}$ of SOM-CSR are updated alternatively as follows.

Step 1) Train filters $\{\mathbf{d}_m\}$ using a pre-given training set.

Step 2) Initial step, $n = 0$: get $\boldsymbol{\xi}_0$ by backpropagation [7], set $\boldsymbol{\alpha}_{j,0} = 0$, and initialize coefficient $\{\mathbf{x}_{m,0}\}$.

Step 3) $n = n + 1$.

Step 3.1) Update $\{\boldsymbol{\alpha}_{j,n}\}$: compute gradient $\mathbf{g}_{j,n} = \bigtriangledown_{\boldsymbol{\alpha}_j} f$; from the derivative $\mathbf{g}_{j,n}$, the next Polak–Ribiere CG search direction $\boldsymbol{\rho}_{j,n} = \mathbf{g}_{j,n} + (\mathrm{Re}[(\mathbf{g}_{j,n} - \mathbf{g}_{j,n-1})^* \cdot \mathbf{g}_{j,n}]/\|\mathbf{g}_{j,n-1}\|_2^2)\boldsymbol{\rho}_{j,n-1}$ can be calculated; the $\boldsymbol{\alpha}$ is updated with a step length $d_{j,n}$ as $\boldsymbol{\alpha}_{j,n} = \boldsymbol{\alpha}_{j,n-1} + d_{j,n}\boldsymbol{\rho}_{j,n}$.

Step 3.2) Update $\{\mathbf{x}_{m,n}\}$ by solving CSC in Eq. (3) with fixed filters $\{\mathbf{d}_m\}$ and $\boldsymbol{\xi}_{n-1}$.

Step 3.3) Update $\boldsymbol{\xi}_n$ from Eq. (4) with fixed $\{\mathbf{x}_{m,n}\}$ and $\boldsymbol{\alpha}_{j,n}$ as

$$(\xi_n)_l = (P_n)_l/(Q_n)_l, \tag{5}$$

where $(\cdot)_l$ represents the lth element of the vector $(\cdot)$,

$$(P_n)_l = \sum_{j=1}^{N_t}\frac{\left(E_{j,n}^{tot}\right)_l^* \cdot \left(I_{j,n}^d\right)_l}{\left\|I_j^s\right\|_2^2} - \frac{iv\eta_0}{k}\cdot\left(\sum_{m=1}^{M}\mathbf{d}_m * \mathbf{x}_{m,n} - 1\right)_l$$

$$(Q_n)_l = \sum_{j=1}^{N_t}\frac{\left(E_{j,n}^{tot}\right)_l^* \cdot \left(I_{j,n}^d\right)_l}{\left\|I_j^s\right\|_2^2} + v\frac{\eta_0^2}{k^2}.$$

Step 4) If the termination condition of maximal iterations (100, as an empirical value by experiments) is satisfied, stop the iteration. Otherwise, go back to step 3).

From Eq. (5), we clearly observe that when the regularization parameter v approaches to zero, the SOM-CSR result is infinitely close to that of SOM. In contrast, it performs like a pure CSC when v becomes infinite.

III. Numerical Results

In this section, we demonstrate the benefit of CSR by comparing the results of SOM-CSR with SOM using both synthetic and experimental data. The root-mean-square error (RMSE) and the structural similarity index measure (SSIM) [24] are used to quantify the reconstruction quality of the two methods.

A. Dictionary learning

In this letter, we take the commonly-used Modified National Institute of Standards and Technology (MNIST) database [25] as the training set to train the filter dictionary. The database is composed of handwritten digits from 0 to 9. To increase the diversity of images, we randomly rotate the digit image with an angle from -170° to 170°, and a random circle is also added in D. We empirically pick 100 random samples with a resolution of 64×64 from this database to train the dictionary filters. According to Eq. (3), the convolutional filters have unitary l^2 norm and they mainly learn prior structural information of unknown scatterers. The range of the relative permittivity has little influence on the training of filters. Thus, we train the filters with all training images with the relative permittivity of scatterers between 1.0 and 1.5. As shown in Fig. 1, the obtained filter dictionary $\{\mathbf{d}_m\}_{m=1}^{32}$ is empirically composed of 32 filters, with each a size of 8×8. The same learned filters will be used by the SOM-CSR method for all the following examples. Meanwhile, the parameter λ for the subsequent CSC in Eq. (3) is always set to 0.03.

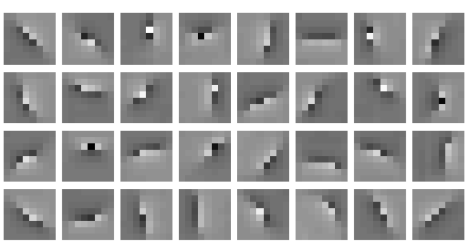

Fig. 1. The dictionary of 32 filters trained with MNIST database.

B. Results of synthetic data

In synthetic examples, the square domain D of size 2.0 m$\times$2.0 m is discretized into 100×100 grids for calculating simulated scattered filed, while the grids of inversion are set to 64×64. The operating frequency is 400 MHz, and there are 16 transmitting antennas and 32 receiving antennas, evenly distributed on a circle S with a radius of 3 m. The regularization parameter v is set to 0.05 for all synthetic examples. We will verify later that the SOM-CSR works well with a relatively large range of v.

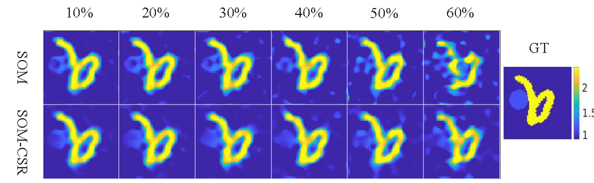

Fig. 2. Reconstruction results of synthetic data from MNIST database (Test#1) by SOM and SOM-CSR, under 10% to 60% Gaussian white noise, respectively.

1) Test with MNIST database: In the first case, we compare the SOM-CSR and SOM with the testing data of another 20 profiles randomly selected from the MNIST database. To evaluate the robustness against noise, we add 10% to 60% Gaussian white noise to the measured scattered field, respectively. The average quality metrics of all comparison results are summarized in Table I. It is found that, although the quality metrics decrease with noise, the SOM-CSR consistently outperforms the SOM. To demonstrate the comparison visually, we show one of the results in Fig. 2, named Test#1, where the GT indicates the profile of ground truth permittivity. The quality metrics of the average results and Test#1 in Table I indicate that the SOM-CSR clearly improves the SSIM, especially for that with high noise levels, while the RMSE is still on a similar level. The results in Test#1 also show that the CSR makes the reconstruction more structural. Finally, the average reconstruction time of a single testing sample in SOM-CSR is 129.30 seconds compared to that of 44.11 seconds in SOM. It should be noted that the CSR can be greatly accelerated by the GPU parallelization as introduced in [26].

TABLE I
Comparison of quality metrics for all reconstruction results and Test#1 in MNIST database under 10% to 60% Gaussian white noise, respectively.

Case	Metric	Method	Noise					
			10%	20%	30%	40%	50%	60%
Average	SSIM	SOM	0.8271	0.7991	0.7618	0.7541	0.7315	0.7116
		SOM-CSR	0.8478	0.8278	0.8008	0.7973	0.7812	0.7713
	RMSE	SOM	0.1463	0.1460	0.1581	0.1669	0.1574	0.1557
		SOM-CSR	0.1443	0.1437	0.1557	0.1633	0.1522	0.1482
Test#1	SSIM	SOM	0.8227	0.8131	0.7903	0.7609	0.7417	0.6173
		SOM-CSR	0.8499	0.8433	0.8368	0.8217	0.8023	0.7512
	RMSE	SOM	0.1393	0.1399	0.1423	0.1491	0.1580	0.2055
		SOM-CSR	0.1382	0.1377	0.1423	0.1455	0.1529	0.1582

2) Test with complex profiles: To test the effectiveness of CSR for reconstructing complex profiles, we further compare the SOM-CSR and SOM methods in Test#2 to Test#4. Particularly, Test#2 is the well-known "*Austria*" [27] profile, where the relative permittivity of scatterers is 2.2. Test#3 is composed of two circles and two rectangles, where the centers of two circles are at (-0.4, 0.6) m and (0.4, 0.6) m, respectively. The radius of each circle is 0.3 m. The center of the rectangle is at (0, -0.3) m, the inner rectangle is 1.0 m long and 0.6 m wide, and the outer one is 1.6 m long and 1.0 m wide. The relative permittivity of the two circles is 2.3, the inner rectangle is 1.6, and the outer rectangle is 1.5. Test#4 consists of two rings, where the radius of the inner circle in the ring is 0.5 m, the radius of the outer circle is 0.7 m, the centers of the two rings are at (0.2, 0.2) m and (-0.2, -0.2) m, respectively, and the relative permittivity is 2.2.

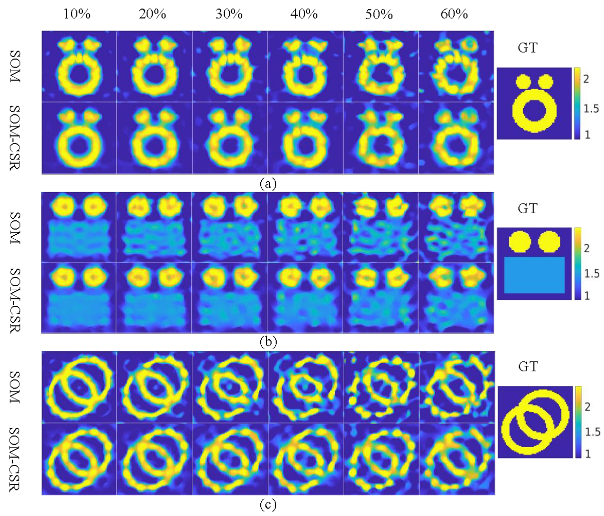

Fig. 3. Reconstruction results of synthetic data with complex profiles by SOM and SOM-CSR, under 10% to 60% Gaussian white noise, respectively. (a) Test#2 (b) Test#3 (c) Test#4.

The reconstruction results of Test#2 to Test#4 are shown in Fig. 3, and the quality metric of SSIM is summarized in Table II. From the results, we observe that the SOM-CSR consistently outperforms the original SOM. The use of CSR makes the reconstruction results of SOM-CSR more robust against noise compared to SOM, which can be clearly observed from the SSIM indices. The reason is that the CSC of target scatterers with learned filters can well recover the structural information. So, it can effectively suppress the interference of white noise compared to the pixel-based inversion.

TABLE II
COMPARISON OF SSIM QUALITY METRICS FOR RECONSTRUCTION RESULTS OF TEST#2-TEST#4 UNDER 10% TO 60% GAUSSIAN WHITE NOISE, RESPECTIVELY.

Case	Metric	Method	Noise					
			10%	20%	30%	40%	50%	60%
Test#2	SSIM	SOM	0.7063	0.6993	0.6709	0.6250	0.6060	0.5723
		SOM-CSR	0.7302	0.7153	0.7012	0.6821	0.6378	0.6201
Test#3	SSIM	SOM	0.6596	0.5489	0.5412	0.4941	0.4195	0.3871
		SOM-CSR	0.7106	0.6698	0.6356	0.6076	0.5404	0.4988
Test#4	SSIM	SOM	0.6889	0.6222	0.5349	0.4513	0.4709	0.4621
		SOM-CSR	0.6951	0.6759	0.6251	0.5863	0.5362	0.5384

C. Test with experimental data

Finally, we verify the SOM-CSR with experimental data provided by Institute Fresnel [28]. The "*FoamDielExt*" profile, named Test#5, is tested by the two methods at the frequency of 3 GHz and 5 GHz, respectively. The DOI D is of size 0.2 m$\times$ 0.2 m, which is discretized into 32×32 grids. Since the regularization parameter v is taken to balance the SOM and CSR in SOM-CSR, we also take this example to explore the effect of v on the overall reconstruction result. The SOM-CSR is tested with different values of v and the SSIM metrics are shown in Fig. 4. It is observed that the SSIM improves as v increases, but the result becomes worse if v is too large. The reason is that the effect of CSR is not significant when v is too small. However, the SOM-CSR degenerates to CSC if v is too large. Fortunately, the reconstruction can be effectively improved when v is in a considerable large range.

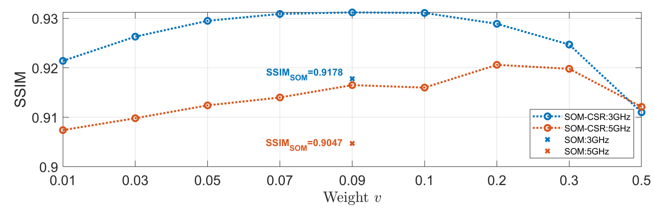

Fig. 4. The SSIM of SOM-CSR reconstructions with different values of v for Fresnel experimental data (Test#5) under 3 GHz and 5 GHz, respectively.

For a detailed comparison, in Fig. 5, we also demonstrate the reconstruction results of SOM-CSR with $v = 0.05$ and $v = 0.2$, respectively. Compared to SOM, there exists a certain improvement on the reconstruction quality of SOM-CSR, which indicates that the CSR is not only effective on simulated data but also the experimental data.

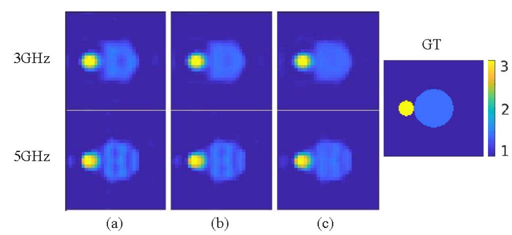

Fig. 5. Reconstruction results of Fresnel experimental data (Test#5) by SOM and SOM-CSR with $v = 0.05$ and $v = 0.2$, respectively. (a) SOM (b) SOM-CSR ($v = 0.05$) (c) SOM-CSR ($v = 0.20$).

IV. CONCLUSION

In this letter, a convolutional sparsity regularization term is proposed, which incorporates prior structural information into nonlinear iterative ISP methods, based on the convolutional sparse coding of scatterers with learned dictionary filters. The CSR has been introduced to work with the subspace optimization algorithm, named SOM-CSR, to enhance the reconstruction quality. Results on synthetic and experimental data have both demonstrated the superior performance of SOM-CSR against noise compared to the original SOM algorithm. Although only verified with SOM, the CSR is expected to also work with other nonlinear iterative methods to improve the quality of ISP reconstructions.

REFERENCES

[1] A. Franchois and C. Pichot, "Microwave imaging-complex permittivity reconstruction with a levenberg-marquardt method," *IEEE Transactions on Antennas and Propagation*, vol. 45, no. 2, pp. 203–215, 1997.

[2] W. C. Chew and Y.-M. Wang, "Reconstruction of two-dimensional permittivity distribution using the distorted Born iterative method," *IEEE Transactions on Medical Imaging*, vol. 9, no. 2, pp. 218–225, 1990.

[3] K. Noritake and S. Kidera, "Boundary extraction enhanced distorted Born iterative method for microwave mammography," *IEEE Antennas and Wireless Propagation Letters*, vol. 18, no. 4, pp. 776–780, 2019.
[4] P. M. Van Den Berg and R. E. Kleinman, "A contrast source inversion method," *Inverse Problems*, vol. 13, no. 6, p. 1607, 1997.
[5] H. Sato and S. Kidera, "ROI limited unknowns reduction based contrast source inversion for microwave breast imaging," *IEEE Antennas and Wireless Propagation Letters*, 2020.
[6] X. Chen, "Subspace-based optimization method for solving inverse-scattering problems," *IEEE Transactions on Geoscience and Remote Sensing*, vol. 48, no. 1, pp. 42–49, 2009.
[7] ——, *Computational methods for electromagnetic inverse scattering*. Wiley Online Library, 2018.
[8] A. Desmal and H. Bağcı, "A preconditioned inexact Newton method for nonlinear sparse electromagnetic imaging," *IEEE Geoscience and Remote Sensing Letters*, vol. 12, no. 3, pp. 532–536, 2014.
[9] ——, "Sparse nonlinear electromagnetic imaging accelerated with projected steepest descent algorithm," *IEEE Transactions on Geoscience and Remote Sensing*, vol. 55, no. 7, pp. 3810–3822, 2017.
[10] A. I. Sandhu, A. Desmal, and H. Bagci, "An accelerated nonlinear contrast source inversion scheme for sparse electromagnetic imaging," *IEEE Access*, vol. 9, pp. 54 811–54 819, 2021.
[11] D. W. Winters, B. D. Van Veen, and S. C. Hagness, "A sparsity regularization approach to the electromagnetic inverse scattering problem," *IEEE Transactions on Antennas and Propagation*, vol. 58, no. 1, pp. 145–154, 2009.
[12] U. Taşkın and Ö. Özdemir, "Sparsity regularized nonlinear inversion for microwave imaging," *IEEE Geoscience and Remote Sensing Letters*, vol. 14, no. 12, pp. 2220–2224, 2017.
[13] L. Zhang, Z. Ma, K. Xu, and Y. Zhong, "Wavelet-based subspace regularization for solving highly nonlinear inverse scattering problems with contraction integral equation," *Electronics*, vol. 9, no. 11, p. 1760, 2020.
[14] L. Pan, X. Chen, and S. P. Yeo, "A compressive-sensing-based phaseless imaging method for point-like dielectric objects," *IEEE Transactions on Antennas and Propagation*, vol. 60, no. 11, pp. 5472–5475, 2012.
[15] R. V. Şenyuva, Ö. Özdemir, G. K. Kurt, and E. Anarım, "Electromagnetic imaging of closely spaced objects using matching pursuit based approaches," *IEEE Antennas and Wireless Propagation Letters*, vol. 15, pp. 1179–1182, 2015.
[16] N. Anselmi, M. Salucci, G. Oliveri, and A. Massa, "Wavelet-based compressive imaging of sparse targets," *IEEE Transactions on Antennas and Propagation*, vol. 63, no. 11, pp. 4889–4900, 2015.
[17] A. Massa, P. Rocca, and G. Oliveri, "Compressive sensing in electromagnetics-a review," *IEEE Antennas and Propagation Magazine*, vol. 57, no. 1, pp. 224–238, 2015.
[18] G. Oliveri, M. Salucci, N. Anselmi, and A. Massa, "Compressive sensing as applied to inverse problems for imaging: Theory, applications, current trends, and open challenges." *IEEE Antennas and Propagation Magazine*, vol. 59, no. 5, pp. 34–46, 2017.
[19] C. Garcia-Cardona and B. Wohlberg, "Convolutional dictionary learning: A comparative review and new algorithms," *IEEE Transactions on Computational Imaging*, vol. 4, no. 3, pp. 366–381, 2018.
[20] M. Aharon, M. Elad, and A. Bruckstein, "K-svd: An algorithm for designing overcomplete dictionaries for sparse representation," *IEEE Transactions on Signal Processing*, vol. 54, no. 11, pp. 4311–4322, 2006.
[21] S. Boyd, N. Parikh, E. Chu, B. Peleato, and J. Eckstein, "Distributed optimization and statistical learning via the alternating direction method of multipliers," *Foundations and Trends in Machine Learning*, vol. 3, no. 1, pp. 1–122, 2010.
[22] B. Wohlberg, "Efficient algorithms for convolutional sparse representations," *IEEE Transactions on Image Processing*, vol. 25, no. 1, pp. 301–315, 2015.
[23] ——, "SPORCO: A python package for standard and convolutional sparse representations," in *Proceedings of the 15th Python in Science Conference, Austin, TX, USA*, 2017, pp. 1–8.
[24] Z. Wang, E. P. Simoncelli, and A. C. Bovik, "Multiscale structural similarity for image quality assessment," in *The Thrity-Seventh Asilomar Conference on Signals, Systems and Computers, 2003*, vol. 2. IEEE, 2003, pp. 1398–1402.
[25] Y. LeCun, L. Bottou, Y. Bengio, and P. Haffner, "Gradient-based learning applied to document recognition," *Proceedings of the IEEE*, vol. 86, no. 11, pp. 2278–2324, 1998.
[26] E. Skau and B. Wohlberg, "A fast parallel algorithm for convolutional sparse coding," in *2018 IEEE 13th Image, Video, and Multidimensional Signal Processing Workshop (IVMSP)*. IEEE, 2018, pp. 1–5.
[27] K. Belkebir and A. Tijhuis, "Using multiple frequency information in the iterative solution of a two-dimensional nonlinear inverse problem," in *Proceedings Progress in Electromagnetics Research Symposium, PIERS 1996, 8 July 1996, Innsbruck, Germany*. Universität Innsbruck, 1996.
[28] J.-M. Geffrin, P. Sabouroux, and C. Eyraud, "Free space experimental scattering database continuation: experimental set-up and measurement precision," *Inverse Problems*, vol. 21, no. 6, p. S117, 2005.